ACS APPLIED MATERIALS & INTERFACES

Research Article

www.acsami.org

Embedding $NiCo_2O_4$ Nanoparticles into a 3DHPC Assisted by CO_2-Expanded Ethanol: A Potential Lithium-Ion Battery Anode with High Performance

Lingyan Wang,[†,‡,§] Linhai Zhuo,*[,∥] Chao Zhang,[†,‡] and Fengyu Zhao*[,†,‡]

[†]State Key Laboratory of Electroanalytical Chemistry, Changchun Institute of Applied Chemistry, and [‡]Laboratory of Green Chemistry and Process, Changchun Institute of Applied Chemistry, Chinese Academy of Sciences, Changchun 130022, People's Republic of China

[§]University of the Chinese Academy of Sciences, Beijing 100049, China

[∥]College of Chemistry and Chemical Engineering, Taishan University, Taian 271021, China

Supporting Information

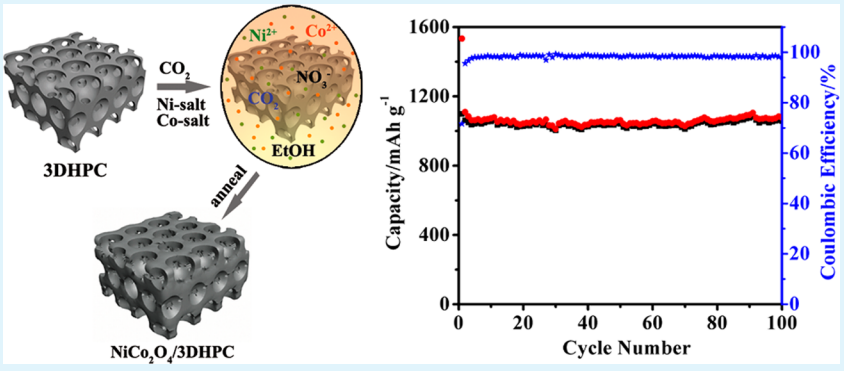

ABSTRACT: A high-performance anode material, $NiCo_2O_4$/3DHPC composite, for lithium-ion batteries was developed through direct nanoparticles nucleation on a three-dimensional hierarchical porous carbon (3DHPC) matrix and cation substitution of spinel Co_3O_4 nanoparticles. It was synthesized via a supercritical carbon dioxide ($scCO_2$) expanded ethanol solution-assisted deposition method combined with a subsequent heat-treatment process. The $NiCo_2O_4$ nanoparticles were uniformly embedded into the porous carbon matrix and efficiently avoided free-growth in solution or aggregation in the pores even at a high content of 55.0 wt %. In particular, the 3DHPC was directly used without pretreatment or surfactant assistance. As an anode material for lithium-ion batteries, the $NiCo_2O_4$/3DHPC composite showed high reversible capacity and improved rate capability that outperformed those composites formed with single metal oxides (NiO/3DHPC, Co_3O_4/3DHPC), their physical mixture, and the composite prepared in pure ethanol ($NiCo_2O_4$/3DHPC-E). The superior performance is mainly contributed to the unique advantages of the $scCO_2$-expanded ethanol medium, and the combination of high utilization efficiency and improved electrical conductivity of $NiCo_2O_4$ as well as the electronic and ionic transport advantages of 3DHPC.

KEYWORDS: *CO_2-expanded ethanol, Ni-doped, hierarchical porous carbon, lithium-ion batteries*

1. INTRODUCTION

To meet the demand for rechargeable lithium-ion batteries (LIBs) with high energy density and power density as well as good cyclability, extensive efforts are in progress to optimize the electrode properties.[1,2] Generally, nanometer-sized electrochemical active materials show improved electrochemical performance due to the increased electrode/electrolyte contact area and short electronic and ionic transport length.[3−5] Meanwhile, it is often necessary to disperse the active materials on a highly conductive and stable carbonaceous nanomaterial to improve the conductivity of composites and meanwhile suppress the self-aggregation during the discharge/charge process.[6] However, there are several intrinsic disadvantages in the conventional solution-based chemical approach, a most common strategy for synthesizing nanostructured composites, such as: (1) A certain amount of precursor cannot deposit onto the matrix and aggregate to free large particles in the solution; it reduces the conductivity of the overall electrode and leads to the active material deactivate quickly. (2) Crystal growth is always involved in the conventional methods, which will inevitably increase the size of the active material. However, the large particle will decrease the electrode/electrolyte contact area when applied for LIBs, increase Li^+ ions diffusion path across the electrode, and cause severe internal stress during

Received: May 7, 2014
Accepted: June 17, 2014
Published: June 17, 2014

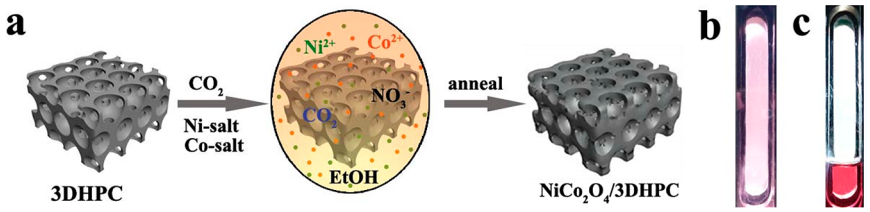

Figure 1. (a) Schematic illustration of the formation of $NiCo_2O_4$/3DHPC composite in $scCO_2$-expanded ethanol solution. Typical phase behavior of the mixed solution of $Ni(NO_3)_2{\cdot}6H_2O$ and $Co(NO_3)_2{\cdot}6H_2O$ in $scCO_2$-expanded ethanol solution (b) and pure ethanol (c).

charge/discharge processes.[7−9] The disadvantages can be partly attributed to the intrinsic properties of solvents, such as high viscosity, the existence of surface tension, and low diffusivity as compared to gases.

As compared to the traditional solvents, supercritical CO_2 ($scCO_2$) exhibits a novel hybrid of gas-like and liquid-like properties; that is, it can dissolve solute like a liquid and yet possesses low viscosity, high diffusivity, and zero surface tension like a gas. These unique properties make $scCO_2$ an attractive medium for delivering reactant molecules to the areas with high aspect ratios, complicated surfaces, and poorly wettable substrates, enabling deposition processes to be controlled quantitatively and uniformly.[10−12] Simultaneously, the loading amount could be precisely tailored by simply varying the concentration of precursors. Furthermore, because the carbonate ions (originated from the reactions of CO_2 and H_2O) participate in nucleation and the intermediates are amorphous,[13] the process of crystal growth could be efficiently avoided, and, consequently, smaller nanoparticles are obtained. In this way, more importantly, the carbon-based matrix could be directly used without pretreatment or surfactant assistance, thus avoiding the damage of morphology and electronic characteristic of primary carbon matrix.[14−16]

In this article, novel $NiCo_2O_4$/3DHPC heteroarchitectures as negative electrodes for high-performance LIBs were fabricated through the $scCO_2$-expanded ethanol-assisted deposition method. With the help of $scCO_2$, small and uniform $NiCo_2O_4$ nanocrystals less than 15 nm were tightly anchored on the macroporous wall of the porous carbon matrix. $NiCo_2O_4$ was chosen as the electrochemical active material due to its better electronic conductivity and richer electrochemical activity as compared to those of nickel oxide (NiO) and cobalt oxide (Co_3O_4).[17−20] Up to now, $NiCo_2O_4$ has gained much research interest in various applications,[21−24] but it was less studied as anode materials for LIBs. The 3DHPC was selected on the basis of its structural advantages, such as the thin wall and interconnected porous structure shorten the diffusion pathways for electrons and ions, and offer sufficient electrode/electrolyte contact area. Moreover, the interconnected structure and the homogeneous coating of more conductive materials provide a three-dimensional, continuous, and fast electronic path in the electrode, which allows faster charge transport.[25−27] When tested as anode materials for LIBs, the prepared $NiCo_2O_4$/3DHPC composite exhibited much higher reversible capacity and significantly improved rate capability. More importantly, it could render reversible capacity of 660 mA h g^{-1}, with 92.3% capacity retention for up to 500 cycles at a current density of 1 A g^{-1}, highlighting its enormous potential in energy management.

2. EXPERIMENTAL SECTION

2.1. Materials. The analytical chemical reagents of $Ni(NO_3)_2{\cdot}6H_2O$, $Co(NO_3)_2{\cdot}6H_2O$, and C_2H_5OH were purchased from Sinopharm Chemical Reagent Beijing Co. Ltd. All of the chemicals were used directly without further purification.

2.2. Synthesis of $NiCo_2O_4$/3DHPC Composites. The 3DHPC matrix was prepared by the procedures described in our previous work.[28] A typical synthesis of $NiCo_2O_4$/3DHPC is as follows: 20 mg of 3DHPC was first dispersed in 10 mL of ethanol solution under ultrasonic treatment for 0.5 h, followed by adding 29 mg of $Ni(NO_3)_2{\cdot}6H_2O$ and 58 mg of $Co(NO_3)_2{\cdot}6H_2O$ into the above solution with magnetic stirring. The resultant solution then was transferred into a 50 mL Teflon-lined stainless-steel high-pressure autoclave, which subsequently was placed into an oil bath at 200 °C, and then CO_2 was pumped up to 12.0 MPa to form a homogeneous expanded fluid with a flow rate of 7 mL min^{-1} under vigorous stirring. The final pressure reached approximately 20 MPa when the temperature reached equilibrium (Caution: Be careful in handling process for scalding and leaking). The autoclave was cooled to room temperature naturally and depressurized slowly after 2 h. The resulting black solid products were centrifuged, washed with ethanol and deionized water, respectively, and then dried at 80 °C in air. Finally, the as-collected samples were calcined at 400 °C for 2 h under N_2 atmosphere. For comparison, NiO/3DHPC and Co_3O_4/3DHPC were prepared under similar conditions, in which the amount of the metal precursor of $Ni(NO_3)_2{\cdot}6H_2O$ or $Co(NO_3)_2{\cdot}6H_2O$ was 87 mg, and the amount of 3DHPC was 20 mg. To elucidate the efficiency of CO_2, $NiCo_2O_4$/3DHPC-E composite was also prepared under the same procedure, where E refers to pure ethanol without introducing CO_2. Additionally, to check the state of the reaction solution, we conducted the visual observation of phase behavior in an 80 mL viewable autoclave, in which 16 mL of ethanol solution of $Ni(NO_3)_2{\cdot}6H_2O$ (46.4 mg) and $Co(NO_3)_2{\cdot}6H_2O$ (92.8 mg) was used, and then introduced CO_2 to 12.0 MPa, and the phase behavior was observed at a reaction temperature of 200 °C.

2.3. Materials Characterization. The crystallite structure and morphologies of the samples were characterized by power X-ray diffraction (XRD, Bruker D8 Advance, Cu Kα radiation, λ = 1.5418 Å), field-emission scanning electron microscopy (FESEM, Hitachi S-4800) equipped with energy-dispersive X-ray spectroscopy (EDX), and transmission electron microscopy (TEM, Tecnai G20). X-ray photoelectron spectroscopy (XPS) was recorded on a PHI quantera SXM spectrometer with an Al Kα = 280.00 eV excitation source. Thermogravimetry analyses (TGA) were performed with a TGA 2050 thermogravimetric analyzer with a ramp rate of 10 °C min^{-1} from room temperature to 800 °C in air. The electrical conductivies were meausured by four-point probe method (Keithely 2400).

2.4. Electrochemical Measurements. The electrochemical tests were measured using two-electrode CR2025 type coin cells. The working electrodes were prepared via a slurry coating procedure. The slurry consisted of active materials (75 wt %), acetylene black (10 wt %), and polyvinylidene fluoride (PVDF, 15 wt %) in *N*-methyl-2-pyrrolidone (NMP). The resultant slurry was pasted onto a pure copper foil, which acted as a current collector. The electrodes were dried at 80 °C for 2 h in air, and then at 120 °C in vacuum overnight and pressed. The mass of every electrode was weighed accurately using an electronic balance. The mass of the active material was controlled in the range of 1−2 mg. Coin cells were assembled in an argon-filled

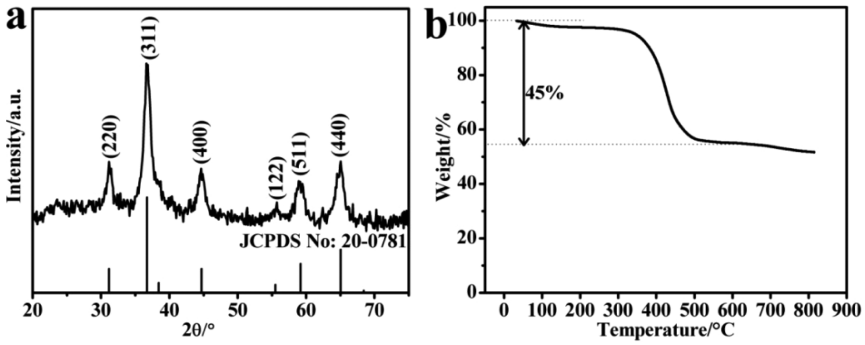

Figure 2. (a) XRD patterns (the bottom line indicates the JCPDS data of $NiCo_2O_4$) and (b) TG curve of the as-prepared $NiCo_2O_4$/3DHPC composite.

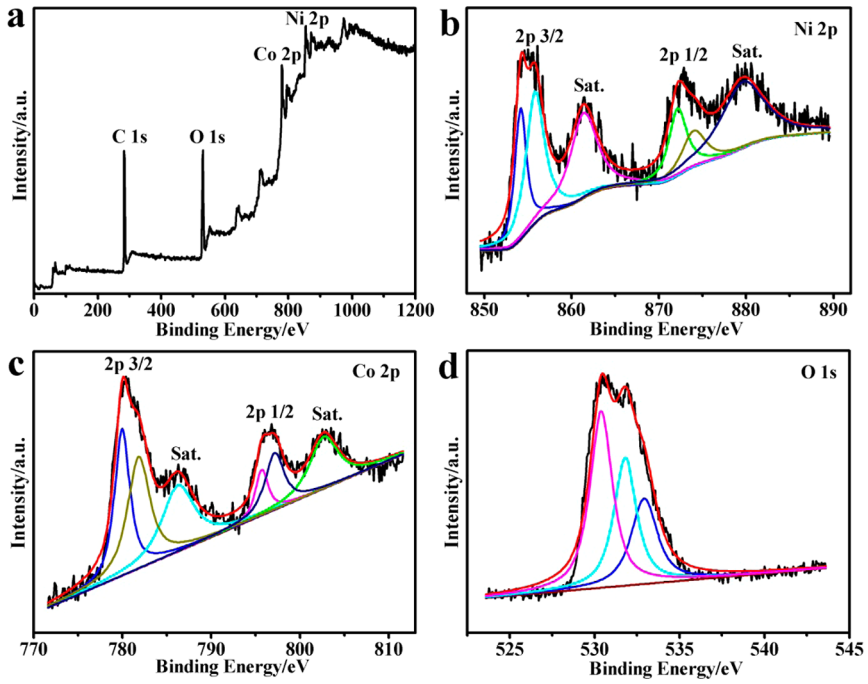

Figure 3. XPS spectra of (a) survey spectrum, (b) Ni 2p, (c) Co 2p, and (d) O 1s for $NiCo_2O_4$/3DHPC composite.

gloved box using lithium sheet as the counter electrode, Celgard 2300 polypropylene as separator, and $LiPF_6$ (1 M) in ethylene carbonate/dimethyl carbonate (EC/DMC, 1:1 in volume) as electrolyte. The galvanostatic charge/discharge tests were performed at various current densities over a voltage range of 0.01−3.0 V (vs Li/Li^+) using a multichannel NEWARE Battery Measurement System (Shenzhen Neware Electronic Co., China). After cycles, the cell was disassembled in the glovebox, and the working electrode was taken out and washed with pure DMC solution for characterizations. Cyclic voltammetry (CV) and electrochemical impedance spectroscopy (EIS) were carried out on an electrochemical workstation (VMP3). Note that the specific capacities of all samples were calculated on the basis of the total weight of the composite.

3. RESULTS AND DISCUSSION

Figure 1a simply illustrates the synthetic procedure of $NiCo_2O_4$ nanoparticles embedded into the 3DHPC. First, the Ni^{2+} and Co^{2+} cations were deposited into 3DHPC matrix in $scCO_2$-expanded ethanol solution, and then the solid precipitate was annealed to the $NiCo_2O_4$/3DHPC composite. Figure 2b shows the phase behavior of the Ni and Co salt in the CO_2-expanded ethanol solution. It is clear that the salt solution was well expanded to form a homogeneous fluid that filled the whole visual vessel in the presence of 12.0 MPa CO_2, in striking contrast to the behavior of the pure ethanol solution (Figure 1c). Consequently, it is believed that $scCO_2$ expanded ethanol solution can disperse hydrous metal nitrates uniformly into the 3DHPC matrix due to its special properties like the low viscosity, high diffusivity, and zero surface tension as compared to the pure ethanol solution, which will be discussed later.

Figure 2a depicts a wide-angle X-ray diffraction (XRD) pattern of the as-prepared $NiCo_2O_4$/3DHPC composite. Well-defined diffraction peaks at 2θ values of 31.1°, 36.7°, 44.6°, 59.1°, and 65.0° are observed, which can be indexed to the lattice plane of (220), (311), (400), (511), and (440) of the spinel $NiCo_2O_4$, respectively, indicating formation of pure $NiCo_2O_4$ crystallites (JCPDS no. 20-0781). The thermogravimetric analysis (TGA) curve of $NiCo_2O_4$/3DHPC (Figure 2b) shows that there is a slight weight loss of about 2.7 wt % before 150 °C, which can be attributed to the absorbed water due to the mesoporous structure of as-prepared sample. About 42 wt % loss in weight presented at 150−800 °C, which is mainly assigned to the combustion of the carbon matrix. The content of $NiCo_2O_4$ in the composite was about 55.0 wt % as estimated from the remnant mass after calcinations in air until 800 °C.

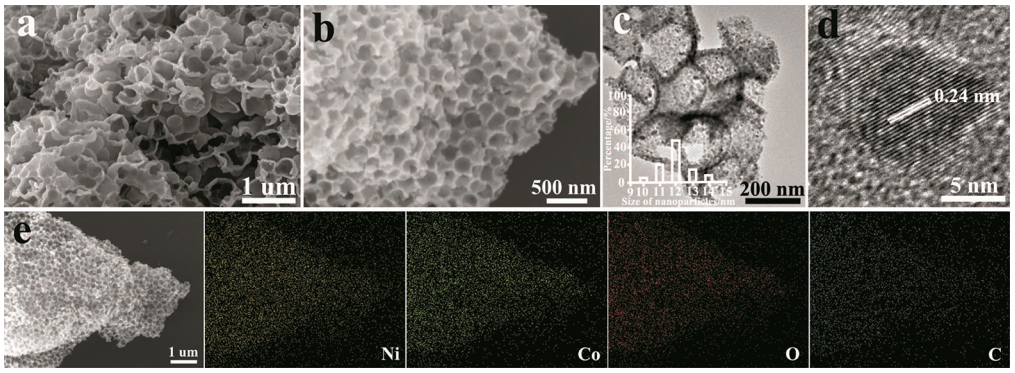

Figure 4. (a,b) SEM, (c) TEM (inset is the size distribution of $NiCo_2O_4$ nanoparticles), (d) HRTEM, and (e) elemental mapping images of $NiCo_2O_4$/3DHPC composite.

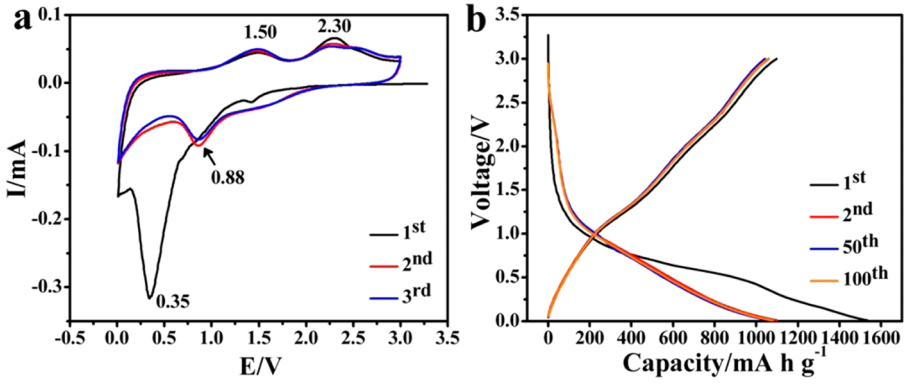

Figure 5. (a) CV curves of $NiCo_2O_4$/3DHPC for the first three cycles at a scan rate of 0.1 mV s^{-1}. (b) The galvanostatic charge/discharge profiles of $NiCo_2O_4$/3DHPC at 100 mA g^{-1}.

To gain more detailed elemental composition and oxidation state of the as-prepared $NiCo_2O_4$/3DHPC composite, X-ray photoelectron spectroscopy (XPS) measurement was operated, and the results are presented in Figure 3. As expected, a full survey of $NiCo_2O_4$/3DHPC reveals the existence of Ni 2p, Co 2p, O 1s, and C 1s (Figure 3a). By using a Gaussian fitting method, the Ni 2p emission spectrum (Figure 3b) was best fitted with two spin−orbit doublets, characteristic of Ni^{2+} and Ni^{3+}, and two shakeup satellite (identified as "Sat."). The Co 2p spectrum (Figure 3c) was also best fitted with two spin−orbit doublets characteristic of Co^{2+} and Co^{3+}, and two shakeup satellites. These results show that the chemical composition of $NiCo_2O_4$ nanoparticles contains Co^{2+}, Co^{3+}, Ni^{2+}, and Ni^{3+}, which are in good agreement with the results in the literature for $NiCo_2O_4$.[29,30] The high-resolution spectrum for the O 1s region (Figure 3d) shows three oxygen contributions. The peak at 530.3 eV is typical O atom in the O−Co/Ni bonding structure. The peak sitting at 531.8 eV is usually associated with defects having low oxygen coordination in the material. Furthermore, the well-resolved peak of 533.0 eV can be attributed to multiplicity of physi- and chemisorbed water on the surface.[31,32]

The morphology and microstructure of all samples were characterized with SEM and TEM. The 3DHPC has regular 3D arrays of interconnected cellular networks (Supporting Information Figure S1a,b). Additionally, the wall of macropores is composed of mutually connected and well-organized mesopores ca. 4 nm in diameter (Supporting Information Figure S1c). It is believed that the unique bimodal pore structure benefits for improving the lithium-storage performance, because the Li^+ ions diffusion strongly depends on the transport length. In comparison to the 3DHPC, the as-prepared $NiCo_2O_4$/3DHPC composite retains the same size and shape as the 3DHPC (Figure 4a,b). From the SEM images, a continuous and uniform $NiCo_2O_4$ layer is coated on the surface of the porous carbon network, and no free $NiCo_2O_4$ particles are formed in the solution. Similarly, the prepared NiO/3DHPC and Co_3O_4/3DHPC composites also show similar appearances (Supporting Information Figure S2a,b). In stark contrast, the $NiCo_2O_4$/3DHPC-E composite obtained in pure ethanol fails to keep the original morphology, showing significant aggregation of $NiCo_2O_4$ on the matrix (Supporting Information Figure S2c). Additionally, for the $NiCo_2O_4$/3DHPC composite (Figure 4c), the $NiCo_2O_4$ particles are nanometer-sized with a narrow size distribution of 11−13 nm and individually embedded into the macropores wall of the 3DHPC with the assistance of $scCO_2$-expanded ethanol solution. HRTEM image confirms the high crystallinity of $NiCo_2O_4$ nanoparticles by a visible set of lattice fringes of 0.24 nm, characteristic of the (311) plane of spinel $NiCo_2O_4$ (Figure 4d). In addition, the elemental mapping images of $NiCo_2O_4$/3DHPC on Ni, Co, O, and C, shown in Figure 4e, obviously demonstrate the uniform dispersion of $NiCo_2O_4$ on the support. Additionally, it was also confirmed in our previous work that the BET surface area and total pore volume of the composite decreased significantly after incorporation of the guess component into the 3DHPC matrix. Nevertheless, the as-prepared composite possessed the same Gaussian pore-size distribution centered at 3.7 nm as that of the 3DHPC matrix by N_2 adsorption−desorption measurements, suggesting that the

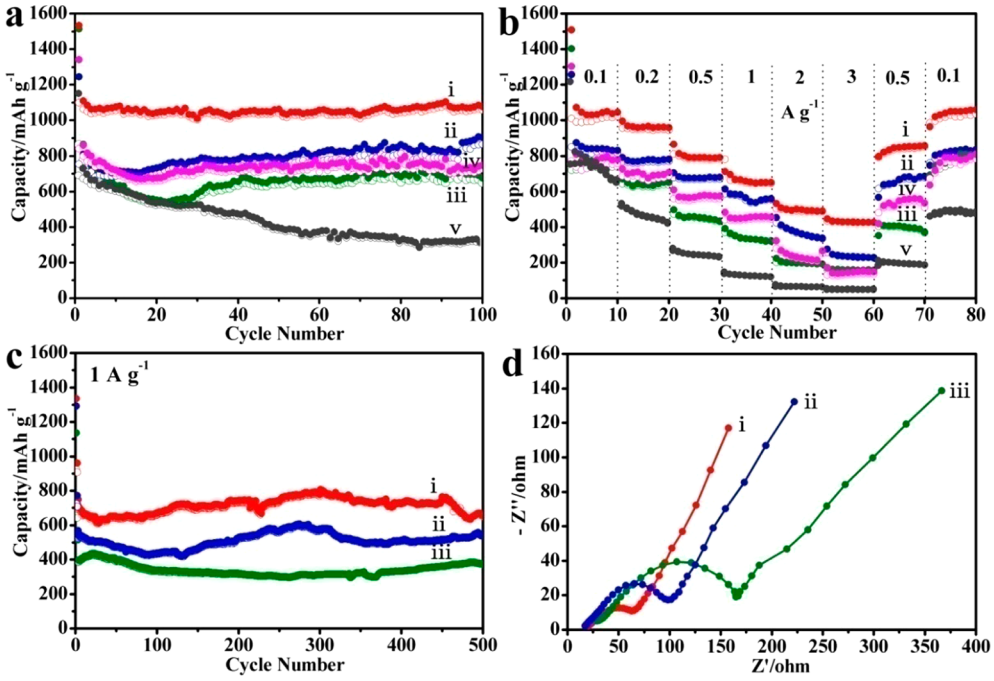

Figure 6. (a) Cycling performance, (b) rate capability, and (c) long-life cycling tests of (i) $NiCo_2O_4$/3DHPC, (ii) Co_3O_4/3DHPC, (iii) NiO/3DHPC, (iv) physical mixture of Co_3O_4/3DHPC and NiO/3DHPC, and (v) $NiCo_2O_4$/3DHPC-E. All of the half-cells were cycled in the potential window from 0.01 to 3.0 V. (d) Nyquist plots of the cycled electrodes after 100 cycles in the frequency range from 100 kHz to 100 mHz.

guess component was mostly anchored on the macropores of the 3DHPC.[28] The above results indicate that $scCO_2$-expanded ethanol is an effective medium for coating the guest components, not only the single metal oxide but also the binary metal oxide, into the matrix with high efficiency.

To evaluate the electrochemical performance of $NiCo_2O_4$/3DHPC as anode materials for LIBs, cyclic voltammetry (CV) and charge/discharge measurements have been conducted. Figure 5a shows the first three CV curves of $NiCo_2O_4$/3DHPC composite. The voltammograms for the first cycle are substantially different from those of the subsequent ones, especially for the discharge branch. In the first cathodic sweep, the intense peak at around 0.35 V corresponds to the reduction of Ni^{3+} or Ni^{2+} and Co^{3+} or Co^{2+} to their metallic states, respectively (eq 1). Also, the reduction peak shifts to a higher potential at 0.88 V in the subsequent cycles. Meanwhile, the two anodic peaks at around 1.50 and 2.30 V could be attributed to the oxidation of Ni^0 to Ni^{2+} and Co^0 to Co^{3+}, respectively (eqs 2–4).[29,33] Apart from the first cycle, the subsequent cycles overlap well, indicating the superior reversibility of the electrochemical reaction. On the basis of the CV result, the entire electrochemical process can be classified as follows:[29,34,35]

$$NiCo_2O_4 + 8Li^+ + 8e^- \rightarrow Ni + 2Co + 4Li_2O \quad (1)$$

$$Ni + Li_2O \rightarrow NiO + 2Li^+ + 2e^- \quad (2)$$

$$Co + Li_2O \rightarrow CoO + 2Li^+ + 2e^- \quad (3)$$

$$CoO + 1/3Li_2O \rightarrow 1/3Co_3O_4 + 2/3Li^+ + 2/3e^- \quad (4)$$

It is proved that $NiCo_2O_4$ offers richer redox reactions than those of the monometallic NiO and Co_3O_4 due to the combined contributions from both nickel and cobalt. It is expected that the $NiCo_2O_4$/3DHPC composite could show enhanced lithium-storage performances.

Figure 5b shows the first, second, 50th, and 100th discharge/charge voltage profiles of $NiCo_2O_4$/3DHPC electrode at a current density of 100 mA g^{-1}. There is an obvious voltage plateau in the first discharge process. The plateau in the consequent discharge curves is slightly higher than that of the first cycle, which is associated with the irreversible reaction of $NiCo_2O_4$ and Li^+ as in eq 1, consistent with the above CV detection results. The initial discharge capacity reaches 1533 mA h g^{-1} (equivalent to ca. 14.0 mol Li per mole of $NiCo_2O_4$), while the charge capacity is 1098 mA h g^{-1}, corresponding to 72% Coulombic efficiency. The large irreversible capacity loss may be related to the formation of SEI film,[36] the generation of LiOH and its reversible decomposition,[37] or simple interfacial storage.[38,39] Although the Coulombic efficiency of the first cycle is low, it is improved greatly, and the value increased to 95.7% at the second cycle, 98% at the 50th and 100th cycles, showing that the irreversible loss reduces upon cycling.

Coin cells with a metallic lithium anode are assembled to investigate the cycling performance and rate capability of the $NiCo_2O_4$/3DHPC. To demonstrate that Ni doping could enhance the electrical conductivity and electrochemical activity of Co_3O_4, we also tested the lithium-storage performance of NiO/3DHPC and Co_3O_4/3DHPC composites obtained under the same experimental conditions in Figure 6. Apparently, $NiCo_2O_4$/3DHPC demonstrated reversible capacity and cycling performance higher than those of NiO/3DHPC and Co_3O_4/3DHPC in Figure 6a. The discharge and charge capacities in the first run are 1533 and 1098 mA h g^{-1} for $NiCo_2O_4$/3DHPC, higher than those of NiO (1513 and 862 mA h g^{-1}) and Co_3O_4 (1244 and 754 mA h g^{-1}). After 100 cycles, the discharge capacity for $NiCo_2O_4$/3DHPC is 1078 mA h g^{-1} with as high as 97% capacity retention, much better than those of NiO (677 mA h g^{-1}, 78%) and Co_3O_4 (906 mA h g^{-1}, 112%). These results show that Ni doping greatly enhances the electrochemical activity and durability of Co_3O_4. Additionally,

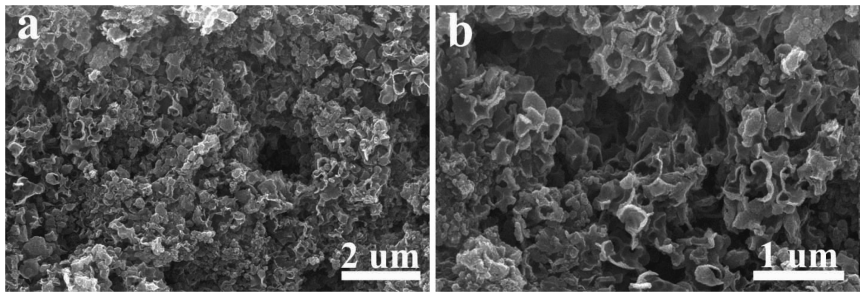

Figure 7. (a,b) SEM images of the cycled $NiCo_2O_4$/3DHPC electrode at different magnifications after 100 cycles at 100 mA g^{-1}.

the physical mixture of equivalent NiO/3DHPC and Co_3O_4/3DHPC composites shows average discharge capacity of 738 mA h g^{-1} with 87% capacity retention at 100 mA g^{-1}. In the case of $NiCo_2O_4$/3DHPC-E composite, its capacity decays rapidly, and only 43% capacity is retained after 100 cycles. With respect to the capacity and cyclability, the striking improvement has been achieved by comparison with the previous result on $NiCo_2O_4$, wherein only 884 mA h g^{-1} was obtained even at the low current of 89 mA h g^{-1}.[40]

To further probe the electrochemical performance of $NiCo_2O_4$/3DHPC composite, we investigated the rate capability of all samples at a current rate range of 0.1−3 A g^{-1}, and then back to 0.5 and 0.1 A g^{-1}. As shown in Figure 6b and Supporting Information Table S1, the $NiCo_2O_4$/3DHPC electrode shows outstanding and fancy rate capability with average discharge capacities of 1046, 966, 792, 652, and 499 mA h g^{-1} at current densities of 0.1, 0.2, 0.5, 1, and 2 A g^{-1}, respectively. Even at a higher rate of 3 A g^{-1}, the discharge capacity still delivers 428 mA h g^{-1}, which is far exceeding those of Co_3O_4/3DHPC (233 mA h g^{-1}), NiO/3DHPC (160 mA h g^{-1}), and $NiCo_2O_4$/3DHPC-E (36 mA h g^{-1}). More importantly, a stable capacity of 1050 mA h g^{-1} (100% of the initial reversible one) can be recovered when the current density returns to 0.1 A g^{-1}. Additionally, the capacities of the physical mixture at various rates are generally located between those of NiO/3DHPC and Co_3O_4/3DHPC, indicating that the lithium-storage performance of $NiCo_2O_4$/3DHPC is not a simple sum of capacities of NiO/3DHPC and Co_3O_4/3DHPC. To our knowledge, the rate performance of $NiCo_2O_4$/3DHPC is comparable to the reported results.[29,33,34,41] The result further confirms the rational configuration of the composite as well as the unique advantages of $scCO_2$ deposition approach.

Considering that a long cycle life at a high current density is one of the key factors for practical LIB application, we further evaluated the $NiCo_2O_4$/3DHPC electrode at a relatively high current density of 1 A g^{-1} up to 500 cycles (Figure 6c). Overall, the $NiCo_2O_4$/3DHPC composite outperforms the Co_3O_4/3DHPC and NiO/3DHPC. The discharge capacity of the $NiCo_2O_4$/3DHPC decreases slightly from 1336 to 627 mA h g^{-1} before the initial 30 cycles. It then tends to increase and stabilize at ca. 720 mA h g^{-1} after 450 cycles. Finally, it remains at 660 mA h g^{-1}; only 7.7% of the original capacitance is lost after 500 cycles. The improved rate performance of the $NiCo_2O_4$/3DHPC composite over Co_3O_4/3DHPC and NiO/3DHPC could be reasonably attributed to the rich redox reactions and the enhanced electrical conductivity. The greatly improved electrical conductivity of $NiCo_2O_4$/3DHPC composite is shown in Supporting Information Table S2, which is consistent with the results in the literature.[42−44] Meanwhile, the electrochemical impedance spectra (EIS) measurements of the cycled electrodes were also tested in Figure 6d. The Nyquist plots show that the diameter of the semicircle for $NiCo_2O_4$/3DHPC electrode in the high-medium frequency region is much smaller than those of Co_3O_4/3DHPC and NiO/3DHPC, suggesting the lower contact and charge-transfer resistance of $NiCo_2O_4$/3DHPC as compared to Co_3O_4/3DHPC and NiO/3DHPC.

The appearance and structure evolution of the $NiCo_2O_4$/3DHPC after 100 discharge/charge cycles were characterized by SEM. The samples were prepared by scraping the active materials from their disks, and then washed with pure DMC solution. The SEM images (Figure 7) show that the morphology and structure of the cycled $NiCo_2O_4$/3DHPC can be generally retained in the whole silhouette. Apparently, there is a cross-linked 3D structure with the presence of numerous spherical cavities. Besides, the surface looks smooth, which may be due to the SEI layer. The above results suggest that the $NiCo_2O_4$ particles are in close contact with the 3DHPC matrix, and the integrity of the composite could be preserved after long-term cycling, holding great potential as a high-rate anode material for lithium storage.

The excellent cycling performance and rate capability of the $NiCo_2O_4$/3DHPC composite could be ascribed to the special architecture, the unique advantages of the $scCO_2$-expanded ethanol medium, and the outstanding electrical conductivity of $NiCo_2O_4$. First, the thin wall and numerous interconnected pores of the $NiCo_2O_4$/3DHPC architecture facilitate diffusion transport for electrons and ions, and offer sufficient electrode/electrolyte contact area for more Li^+ migration across the interface, thus leading to the high specific capacity. Second, the present synthetic method makes almost all of the $NiCo_2O_4$ particles well disperse rather than aggregate, thereby enhancing the utilization efficiency of $NiCo_2O_4$ on specific capacitance and relieving the strain induced by the volume change during charging/discharging. Third, the well-established interconnection of the carbon substrate and active $NiCo_2O_4$ enables fast electron transfer within the hybrid electrode, leading to the low internal resistance and allowing faster charge transport, which is especially important for improving the electrochemical performance of LIBs. Finally, the addition of Ni species into the spinel lattice creates highly efficient active sites and increases the electrical conductivity, which is highly desirable for fast charge transfer.

4. CONCLUSIONS

A novel $NiCo_2O_4$/3DHPC composite was developed as superior anode materials for LIBs by combining nanoparticles direct nucleation on 3DHPC and cation substitution of spine metal oxide nanoparticles. The adopted $scCO_2$-expanded ethanol-assisted deposition technique successfully embedded

11−13 nm $NiCo_2O_4$ nanoparticles into the 3DHPC matrix without pretreatment or surfactant assistance, and effectively avoided free-growth or agglomeration of $NiCo_2O_4$ nanoparticles. At the same mass loading, the $NiCo_2O_4$/3DHPC composite can outperform the composites formed with single metal oxides (NiO/3DHPC, Co_3O_4/3DHPC), their physical mixture, and $NiCo_2O_4$/3DHPC-E composite. The excellent electrochemical performance could be ascribed to the unique advantages of the $scCO_2$-expanded ethanol medium and the rational combination of the merits of $NiCo_2O_4$ and 3DHPC. Meanwhile, because the present synthetic method is simple and of high-efficiency, it provides a new route to design and synthesize functional hybrid nanomaterials for different applications.

■ ASSOCIATED CONTENT

Supporting Information

SEM images of 3DHPC, NiO/3DHPC, Co_3O_4/3DHPC, and $NiCo_2O_4$/3DHPC-E; electrochemical data and electrical conductivity of all samples. This material is available free of charge via the Internet at http://pubs.acs.org.

■ AUTHOR INFORMATION

Corresponding Authors

*Tel./fax: +86-431-85262410. E-mail: zhuoling77@163.com.
*E-mail: zhaofy@ciac.ac.cn.

Notes

The authors declare no competing financial interest.

■ ACKNOWLEDGMENTS

This work was financially supported by the One Hundred Talent Program of CAS and NSFC (21273222).

■ REFERENCES

(1) Liu, C.; Li, F.; Ma, L. P.; Cheng, H. M. Advanced Materials for Energy Storage. *Adv. Energy Mater.* **2010**, *22*, E28−E62.
(2) Bruce, P. G.; Scrosati, B.; Tarascon, J. M. Nanomaterials for Rechargeable Lithium Batteries. *Angew. Chem., Int. Ed.* **2008**, *47*, 2930−2946.
(3) Hu, Y. S.; Kienle, L.; Guo, Y. G.; Maier, J. High Lithium Electroactivity of Nanometer-Sized Rutile TiO_2. *Adv. Mater.* **2006**, *18*, 1421−1426.
(4) Poizot, P.; Laruelle, S.; Grugeon, S.; Dupont, L.; Tarascon, J. M. Nano-Sized Transition-Metal Oxides as Negative-Electrode Materials for Lithium-Ion Batteries. *Nature* **2000**, *407*, 496−499.
(5) Balaya, P. Size Effects and Nanostructured Materials for Energy Applications. *Energy Environ. Sci.* **2008**, *1*, 645−654.
(6) Lee, J. E.; Yu, S. H.; Lee, D. J.; Lee, D. C.; Han, S. I.; Sung, Y. E.; Hyeon, T. Facile and Economical Synthesis of Hierarchical Carbon-Coated Magnetite Nanocomposite Particles and Their Applications in Lithium Ion Battery Anodes. *Energy Environ. Sci.* **2012**, *5*, 9528−9533.
(7) Wu, Z. S.; Ren, W. C.; Wen, L.; Gao, L. B.; Zhao, J. P.; Chen, Z. P.; Zhou, G. M.; Li, F.; Cheng, H. M. Graphene Anchored with Co_3O_4 Nanoparticles as Anode of Lithium Ion Batteries with Enhanced Reversible Capacity and Cyclic Performance. *ACS Nano* **2010**, *4*, 3187−3194.
(8) Su, Y. Z.; Li, S.; Wu, D. Q.; Zhang, F.; Liang, H. W.; Gao, P. F.; Cheng, C.; Feng, X. L. Two-Dimensional Carbon-Coated Graphene/Metal Oxide Hybrids for Enhanced Lithium Storage. *ACS Nano* **2012**, *6*, 8349−8356.
(9) He, C. N.; Wu, S.; Zhao, N. Q.; Shi, C. S.; Liu, E. Z.; Li, J. J. Carbon-Encapsulated Fe_3O_4 Nanoparticles as a High-Rate Lithium Ion Battery Anode Material. *ACS Nano* **2013**, *7*, 4459−4469.
(10) Cooper, A. I. Porous Materials and Supercritical Fluids. *Adv. Mater.* **2003**, *15*, 1049−1059.
(11) Eckert, C. A.; Knutson, B. L.; Debenedetti, P. G. Supercritical Fluids as Solvents for Chemical and Materials Processing. *Nature* **1996**, *383*, 313−318.
(12) Ye, X. R.; Lin, Y. H.; Wang, C. M.; Engelhard, M. H.; Wang, Y.; Wai, C. M. Supercritical Fluid Synthesis and Characterization of Catalytic Metal Nanoparticles on Carbon Nanotubes. *J. Mater. Chem.* **2004**, *14*, 908−913.
(13) Ming, J.; Wu, C. Y.; Cheng, H. Y.; Yu, Y. C.; Zhao, F. Y. Reaction of Hydrous Inorganic Metal Salts in CO_2 Expanded Ethanol: Fabrication of Nanostructured Materials via Supercritical Technology. *J. Supercrit. Fluids* **2011**, *57*, 137−142.
(14) Liu, Z. M.; Han, B. X. Synthesis of Carbon-Nanotube Composites Using Supercritical Fluids and Their Potential Applications. *Adv. Mater.* **2009**, *13*, 825−829.
(15) Sun, Z. Y.; Zhang, X. R.; Han, B. X.; Wu, Y. Y.; An, G. M.; Liu, Z. M.; Miao, S. D.; Miao, Z. J. Coating Carbon Nanotubes with Metal Oxides in a Supercritical Carbon Dioxide-Ethanol Solution. *Carbon* **2007**, *45*, 2589−2596.
(16) Ming, J.; Cheng, H. Y.; Yu, Y. C.; Wu, Y. Q.; Zhao, F. Y. A New Strategy for Finely Controlling the Metal (Oxide) Coating on Colloidal Particles with Tunable Catalytic Properties. *J. Mater. Chem.* **2011**, *21*, 6654−6659.
(17) Li, L. L.; Peng, S. J.; Cheah, Y. L.; Teh, P. F.; Wang, J.; Wee, G.; Ko, Y. W.; Wong, C. L.; Srinivasan, M. Electrospun Porous $NiCo_2O_4$ Nanotubes as Advanced Electrodes for Electrochemical Capacitors. *Chem.—Eur. J.* **2013**, *19*, 5892−5898.
(18) Liu, M. C.; Kong, L. B.; Lu, C.; Li, X. M.; Luo, Y. C.; Kang, L.; Li, X. H.; Walsh, F. C. A Sol-Gel Process for the Synthesis of $NiCo_2O_4$ Having Improved Specific Capacitance and Cycle Stability for Electrochemical Capacitors. *J. Electrochem. Soc.* **2012**, *159*, A1262−A1266.
(19) Yu, L.; Zhang, G. Q.; Yuan, C. Z.; Lou, X. W. Hierarchical $NiCo_2O_4$@MnO_2 Core-Shell Heterostructured Nanowire Arrays on Ni Foam as High-Performance Supercapacitor Electrodes. *Chem. Commun.* **2013**, *49*, 137−139.
(20) Jiang, H.; Ma, J.; Li, C. Z. Hierarchical Porous $NiCo_2O_4$ Nanowires for High-Rate Supercapacitors. *Chem. Commun.* **2012**, *48*, 4465−4467.
(21) Zhang, L. X.; Zhang, S. L.; Zhang, K. J.; Xu, G. J.; He, X.; Dong, S. M.; Liu, Z. H.; Huang, C. S.; Gu, L.; Cui, G. L. Mesoporous $NiCo_2O_4$ Nanoflakes as Electrocatalysts for Rechargeable Li-O_2 Batteries. *Chem. Commun.* **2013**, *49*, 3540−3542.
(22) Xiao, Y.; Hu, C. G.; Qu, L. T.; Hu, C. W.; Cao, M. H. Three-Dimensional Macroporous NiCo2O4 Sheets as a Non-Noble Catalyst for Efficient Oxygen Reduction Reactions. *Chem.—Eur. J.* **2013**, *19*, 14271−14278.
(23) Deng, F. Z.; Yu, L.; Cheng, G.; Lin, T.; Sun, M.; Ye, F.; Li, Y. F. Synthesis of Ultrathin Mesoporous $NiCo_2O_4$ Nanosheets on Carbon Fiber Paper as Integrated High-Performance Electrodes for Supercapacitors. *J. Power Sources* **2014**, *251*, 202−207.
(24) Liu, X. Y.; Shi, S. J.; Xiong, Q. Q.; Li, L.; Zhang, Y. J.; Tang, H. P.; Gu, C. D.; Wang, X. L.; Tu, J. P. Hierarchical $NiCo_2O_4$@$NiCo_2O_4$ Core/Shell Nanoflake Arrays as High-Performance Supercapacitor Materials. *ACS Appl. Mater. Interfaces* **2013**, *5*, 8790−8795.
(25) Estevez, L.; Dua, R.; Bhandari, N.; Ramanujapuram, A.; Wang, P.; Giannelis, E. P. A Facile Approach for the Synthesis of Monolithic Hierarchical Porous Carbons - High Performance Materials for Amine Based CO_2 Capture and Supercapacitor Electrode. *Energy Environ. Sci.* **2013**, *6*, 1785−1790.
(26) Huang, X.; Yu, H.; Chen, J.; Lu, Z. Y.; Yazami, R.; Hng, H. H. Ultrahigh Rate Capabilities of Lithium-Ion Batteries from 3D Ordered Hierarchically Porous Electrodes with Entrapped Active Nanoparticles Configuration. *Adv. Mater.* **2014**, *26*, 1296−1303.
(27) Chou, T. C.; Doong, R. A.; Hu, C. C.; Zhang, B. S.; Su, D. S. Hierarchically Porous Carbon with Manganese Oxides as Highly Efficient Electrode for Asymmetric Supercapacitors. *ChemSusChem* **2014**, *7*, 841−847.
(28) Wang, L. Y.; Zhuo, L. H.; Zhang, C.; Zhao, F. Y. Supercritical Carbon Dioxide Assisted Deposition of Fe_3O_4 Nanoparticles on

Hierarchical Porous Carbon and Their Lithium-Storage Performance. *Chem.—Eur. J.* **2014**, *20*, 4308−4315.
(29) Li, J. F.; Xiong, S. L.; Liu, Y. R.; Ju, Z. C.; Qian, Y. T. High Electrochemical Performance of Monodisperse $NiCo_2O_4$ Mesoporous Microspheres as an Anode Material for Li-Ion Batteries. *ACS Appl. Mater. Interfaces* **2013**, *5*, 981−988.
(30) Lee, D. U.; Kim, B. J.; Chen, Z. W. One-Pot Synthesis of a Mesoporous $NiCo_2O_4$ Nanoplatelet and Graphene Hybrid and Its Oxygen Reduction and Evolution Activities as an Efficient Bi-Functional Electrocatalyst. *J. Mater. Chem. A* **2013**, *1*, 4754−4762.
(31) Yuan, C. Z.; Li, J. Y.; Hou, L. R.; Zhang, X. G.; Shen, L. F.; Lou, X. W. Ultrathin Mesoporous $NiCo_2O_4$ Nanosheets Supported on Ni Foam as Advanced Electrodes for Supercapacitors. *Adv. Funct. Mater.* **2012**, *22*, 4592−4597.
(32) Liu, Z. Q.; Xiao, K.; Xu, Q. Z.; Li, N.; Su, Y. Z.; Wang, H. J.; Chen, S. Fabrication of Hierarchical Flower-Like Super-Structures Consisting of Porous $NiCo_2O_4$ Nanosheets and Their Electrochemical and Magnetic Properties. *RSC Adv.* **2013**, *3*, 4372−4380.
(33) NuLi, Y. N.; Zhang, P.; Guo, Z. P.; Liu, H. K.; Yang, J. $NiCo_2O_4$/C Nanocomposite as a Highly Reversible Anode Material for Lithium-Ion Batteries. *Electrochem. Solid-State Lett.* **2008**, *11*, A64−A67.
(34) Chen, Y. J.; Zhu, J.; Qu, B. H.; Lu, B. A.; Xu, Z. Graphene Improving Lithium-Ion Battery Performance by Construction of $NiCo_2O_4$/Graphene Hybrid Nanosheet Arrays. *Nano Energy* **2014**, *3*, 88−94.
(35) Guo, H.; Liu, L. X.; Li, T. T.; Chen, W. W.; Liu, J. J.; Guo, Y. Y.; Guo, Y. C. Accurate Hierarchical Control of Hollow Crossed $NiCo_2O_4$ Nanocubes for Superior Lithium Storage. *Nanoscale* **2014**, *6*, 5491−5497.
(36) Goodenough, J. B.; Park, K. S. The Li-Ion Rechargeable Battery: a Perspective. *J. Am. Chem. Soc.* **2013**, *135*, 1167−1176.
(37) Hu, Y. Y.; Liu, Z.; Nam, K. W.; Borkiewicz, O. J.; Cheng, J.; Hua, X.; Dunstan, M. T.; Yu, X.; Wiaderek, K. M.; Du, L. S.; Chapman, K. W.; Chupas, P. J.; Yang, X. Q.; Grey, C. P. Origin of Additional Capacities in Metal Oxide Lithium-Ion Battery Electrodes. *Nat. Mater.* **2013**, *12*, 1130−1136.
(38) Laruelle, S.; Grugeon, S.; Poizot, P.; Dollé, M.; Dupont, L.; Tarascon, J. M. On the Origin of the Extra Electrochemical Capacity Displayed by MO/Li Cells at Low Potential. *J. Electrochem. Soc.* **2002**, *149*, A627−A634.
(39) Ponrouch, A.; Taberna, P. L.; Simon, P.; Palacín, M. R. On the Origin of the Extra Capacity at Low Potential in Materials for Li Batteries Reacting Through Conversion Reaction. *Electrochim. Acta* **2012**, *61*, 13−18.
(40) Alcantara, R.; Jaraba, M.; Lavela, P.; Tirado, J. L. $NiCo_2O_4$ Spinel: First Report on a Transition Metal Oxide for the Negative Electrode of Sodium-Ion Batteries. *Chem. Mater.* **2002**, *14*, 2847−2848.
(41) Huang, G.; Zhang, L. L.; Zhang, F. F.; Wang, L. M. Metal-Organic Framework Derived Fe_2O_3@$NiCo_2O_4$ Porous Nanocages as Anode Materials for Li-Ion Batteries. *Nanoscale* **2014**, *6*, 5509−5515.
(42) Appandairajan, N. K.; Gopalakrishnan, J. A Study of $Co_{3-x}Ni_xO_4$ ($0 \leq x \leq 1$) System. *Proc. Indian Acad. Sci.* **1978**, *87*, 115−120.
(43) Li, Y.; Hasin, P.; Wu, Y. Y. $Ni_xCo_{3-x}O_4$ Nanowire Arrays for Electrocatalytic Oxygen Evolution. *Adv. Mater.* **2010**, *22*, 1926−1929.
(44) Liu, J.; Liu, C. P.; Wan, Y. L.; Liu, W.; Ma, Z. S.; Ji, S. M.; Wang, J. B.; Zhou, Y. C.; Hodgson, P.; Li, Y. C. Facile Synthesis of $NiCo_2O_4$ Nanorod Arrays on Cu Conductive Substrates as Superior Anode Materials for High-Rate Li-Ion Batteries. *CrystEngComm* **2013**, *15*, 1578−1585.